ISSN 1995-0780, Nanotechnologies in Russia, 2020, Vol. 15, No. 1, pp. 105–111. © Pleiades Publishing, Ltd., 2020.
Russian Text © The Author(s), 2020, published in Rossiiskie Nanotekhnologii, 2020, Vol. 15, No. 1.

NANOBIOMEDICINE AND NANOPHARMACEUTICALS

X-Ray Nanophosphors Based on $BaGdF_5$ for X-Ray Photodynamic Therapy in Oncology

D. Yu. Kirsanova[a,*], V. V. Butova[a], V. A. Polyakov[a], P. V. Zolotukhin[a], A. A. Belanova[a], V. M. Legostaev[b], E. A. Kuchma[a,b], Z. M. Gadzhimagomedova[a], and A. V. Soldatov[a]

[a] *The Smart Materials Research Institute, Southern Federal University, Rostov-on-Don, 344090 Russia*

[b] *National Medical Research Center for Oncology, Rostov-on-Don, 344037 Russia*

**e-mail: dkirs27@gmail.com*

Received April 29, 2020; revised May 29, 2020; accepted May 29, 2020

Abstract—X-ray and gamma radiation can be used to expand the possibilities of photodynamic therapy in the treatment of deep-lying tumors. One of the promising materials for converting X-ray radiation to optical radiation is $BaGdF_5$ nanoparticles doped with ions of rare-earth elements. It is shown that solvothermal synthesis and a technique using microwave radiation lead to the production of $BaGdF_5$:Eu nanoparticles with similar characteristics; however, when using microwave radiation, the time of the synthesis decreases by at least an order of magnitude. Microwave-synthesized doped $BaGdF_5$:Eu nanoparticles are biocompatible and in terms of size (6–14 nm) meet the requirements for the subsequent preparation of nanocomposites based on them with the optical photosensitizers necessary for X-ray photodynamic therapy.

DOI: 10.1134/S1995078020010164

INTRODUCTION

Morbidity and mortality in malignant neoplasms is one of the most socially significant problems both in Russia and abroad. According to the World Health Organization (WHO), the total number of deaths from cancer in the European Union (EU) were 1 283 101 in 2012 [1]. To date, the world has developed many approaches such as oncology to treat this disease. The traditional methods of treating malignant tumors are surgery, radiotherapy, chemotherapy, or their combination. The disadvantage of these methods is the large number of complications and high mortality rate. Photodynamic therapy (PDT) appeared as an alternative treatment for cancer and is considered the least invasive method compared to chemotherapy and radiation therapy. Photodynamic therapy includes three main components: a photosensitive substance (photosensitizer, PS), oxygen, and light. Two components, PS and light, are external factors. The third necessary component of the photodynamic reaction is an endogenous factor: oxygen. The photosensitizer is injected into the patient and then selectively accumulates in the tumor. The next stage is the irradiation of the tumor tissue with visible or near-infrared light of a certain wavelength necessary for the activation of the PS, which leads to the formation of the reactive oxygen species (ROS) [2]. The active form of oxygen is a group of highly active chemicals that alter some components of the tumor's stroma and ultimately destroy the cancer cells [3] that have a higher level of oxidation compared to normal cells [4]. It is well known that singlet oxygen $^1O_2$ is a key cytotoxic agent in PDT; however, it has been suggested that other free radicals may play a major role in photodynamic cell damage [5]. Using PDT allows us to ensure the maximum number of healthy cells, treat patients without surgical intervention, and reduce the number of complications. However, with all the advantages of PDT, its use for the treatment of deep neoplasms is ineffective. The problem lies in the difficulty of the radiation of the optical range penetrating deep into the tissues. The traditional visible light used in PDT (spectral range 400–700 nm) is limited to surface lesions and the penetration depth of light does not exceed 1 cm. This leads to the fact that during normal PDT only surface tumors can be treated. Therefore, researchers are trying to increase the efficiency of PDT, especially by searching for new sources of deeper radiation [6].

In order to increase the depth of light penetration and activate the PDT process in deep tissues, X rays or gamma rays can be used as the radiation source [7]. This technique, called X-ray photodynamic therapy (XPDT), has great potential for the treatment of tumors of the internal organs. This therapy is carried out according to the same scheme as PDT but it is based on the use of X-ray nanoluminophores (scintillating nanoparticles), which, under the influence of ionizing (in this case, X-ray) radiation, emit light in the visible region, which activates the conjugated PS

Table 1. Details of the synthesis of samples of X-ray nanophosphors

Sample designation	Synthesis method	Synthesis conditions		Precursor molar ratio		
		time, h	*t*, °C	Ba	Gd	Eu
$BaGdF_5$:Eu-ST	ST	24	200	1	0.9	0.1
$BaGdF_5$:Eu-MW	MW	2	200	1	0.9	0.1

ST, solvothermal method; MW, microwave.

through a fluorescence resonant energy transfer and leads to the generation of ROS.

Most often, in the scientific literature, the use of luminescent materials based on the radiation of rare-earth ions for XPDT is found [8]. For example, rare-earth fluoride nanoparticles (such as $BaGdF_5$) are most interesting and studied as the base material for alloying with rare-earth ions (Eu^{3+}, Sm^{3+}, etc.). This is due to the fact that $BaGdF_5$ nanoparticles have a low degree of toxicity, low phonon energy, multicolor tunable luminescence, and strong resistance to photobleaching and photochemical decomposition [9]. This material family has tunable luminescence characteristics [10–12] and fairly good biocompatibility [13]. They are also capable of effectively converting ionizing radiation into the visible or ultraviolet region due to the stepwise multiphoton process that occurs in the system of the energy levels of rare-earth ions that are built into the crystal lattice of the main substance [14, 15]. In addition, the redox stability of the lanthanide ions Ln^{3+} makes them suitable for use in biological tissue cells [16, 17], including human red blood cells [18]. However, some researchers consider nanoparticles based on $NaGdF_4$:Eu^{3+} more promising for XPDT [19].

In this paper, we present a new method for the synthesis of X-ray nanophosphors for XPDT based on $BaGdF_5$ nanoparticles using a microwave reactor, and the possibility of doping this material with a rare-earth element Eu^{3+} is also studied. The characteristics of the obtained nanoparticles, including their cytotoxicity, was studied in detail.

MATERIALS AND METHODS

Starting materials: gadolinium (III) chloride $GdCl_3$, europium (III) chloride $EuCl_3$, ethylene glycol, barium chloride dihydrate $BaCl_2 \cdot 2H_2O$, polyethylene glycol (PEG, $M = 1500$ g/mol), and ammonium fluoride NH_4F.

The synthesis was carried out using two methods. The solvothermal method was adapted from the work [20]. Based on it, in this study, a new microwave synthesis of this material was developed. Details of the synthesis of samples of X-ray nanophosphors are presented in Table 1.

In order to obtain $BaGdF_5$:Eu-ST and $BaGdF_5$:Eu-MW samples 0.9 mmol (237.2 mg) of gadolinium (III) chloride and 0.1 mmol (25.8 mg) of europium (III) chloride were dissolved in 20 mL of ethylene glycol under ultrasound (10 min). Then, 1 mmol (244.2 mg) of barium chloride dihydrate was added to the resulting solution, and the resulting mixture was stirred for 30 minutes. After this, 1.5 g of PEG was added to the mixture and sonication was performed for 15 min. A solution of 5.5 mmol (203.7 mg) of ammonium fluoride in 10 mL of ethylene glycol was separately prepared. The mixture was thoroughly mixed and sonicated for 30 minutes.

Further, in the case of the synthesis of the $BaGdF_5$:Eu-ST sample, the resulting suspension was transferred into a Teflon glass of a steel autoclave, hermetically closed, and incubated for 24 h at a temperature of 200°C.

In order to obtain a sample of $BaGdF_5$:Eu-MW, the resulting suspension was transferred to a Teflon ampoule and placed in a CEM Mars6 microwave oven. The reaction mixture was heated to 200°C for 20 min, then kept at this temperature for 2 h. The used power of the microwave reactor was 600 watts.

The resulting precipitates were washed thrice with distilled water by centrifugation and then dried at 60°C.

X-ray powder diffraction data were obtained using a D2 Phaser diffractometer (Bruker, United States). The shape and size of the particles were studied using transmission electron microscopy (TEM) using a Tecnai G2 Spirit BioTWIN microscope (FEI, United States). The elemental composition was monitored using an M4 Tornado 2D X-ray microfluorescence spectrometer (Bruker, United States).

The cytotoxicity and the effect of the studied nanomaterials on the oxidative status of cells were analyzed on the human cells of the HeLa and K562 lines. The cells were cultured in 24-well plates (SPL Lifesciences, South Korea) in a GlutaMax DMEM (Thermo Fisher Scientific, United States) medium supplemented with 10% fetal bovine serum (GE Healthcare, United Kingdom), 50 IU/mL penicillin, and 50 μg/mL of streptomycin (Thermo Fisher Scientific, United States). The cells were incubated at 37°C and 5% carbon dioxide in a Sanyo MCO-18AC incubator (Panasonic, Japan). The condition of the culture

was evaluated using an inverted Premiere MIS-9000 microscope (C&A, China).

To analyze the cytotoxicity of the materials on the HeLa cells, a trypan blue test was performed with an assessment on a Countess II FL automatic cell viability analyzer according to the manufacturer's protocol (Thermo Fisher Scientific, United States). During the experiment, the stock solution of the nanomaterial in the saline was introduced into the culture medium to the final concentration of 50 μg/mL. In the control group, instead of the solution of the nanomaterial, the saline was administered. Incubation in both groups was performed for 24 h.

Flow cytometry was performed on the K562 cells. The cells were incubated with nanomaterial analogously to the cytotoxicity experiment, but for one hour. The analysis was performed on a CytoFlex flow cytometer (Beckman Coulter, United States) using the following molecular probes:

—CellRox Green: probe for ROS mitochondria and nuclei;

—CellRox Orange: probe for cytosolic ROS;

—7-AAD: control dye for detecting analysis of a population of living cells.

All the dyes were used in accordance with the manufacturer's recommendations (Thermo Fisher Scientific, United States). At least 10 000 events were analyzed in each sample. The analysis included only events morphologically characterized as live singlets of moderate granulation—with gating on channels FSC-A, SSC-A, FSC-H, and 7-AAD.

The signal from the molecular probes was normalized by the direct light scattering channel.

DISCUSSION

X-ray diffraction. As can be seen from the profiles of powder X-ray diffraction, the synthesized samples of $BaGdF_5$:Eu-ST and $BaGdF_5$:Eu-MW are single-phase materials with a structure similar to the published data. The broadening of the peaks is due to the small particle size. Using the Jana2006 program for the $BaGdF_5$:Eu-ST and $BaGdF_5$:Eu-MW samples, the unit cell parameters were calculated at 5.930 (3) and 5.9431 (19) Å, respectively. These values were less than parameter $a = 6.023$ Å declared in the literature for $BaGdF_5$ [21]. This explains the fact that with the partial replacement of Gd^{3+} by Eu^{3+} a shift of the peaks to the high-angle region is observed, which in turn corresponds to a decrease in the unit cell parameter.

Thus, the use of the standard solvothermal method and the method using microwave radiation leads to the formation of nanoparticles that resemble each other in their structural data; however, the time of the synthesis using microwave radiation is more than an order of magnitude shorter than in the standard solvothermal approach, which corresponds to the previously obtained results for the synthesis of other classes of nanoparticles [22, 23].

The results of electron microscopy. The obtained materials $BaGdF_5$:Eu-ST and $BaGdF_5$:Eu-MW are spherical particles 4–14 nm in size (Figs. 2a, 2b), which fully complies with the requirements for the production of nanocomposites for the XPDT based on them, which should combine the nanoluminophores and PS nanoparticles [24, 25]. The size distribution of the nanoparticles was estimated using the TEM data; moreover, 760 $BaGdF_5$:Eu-ST particles and 1140 $BaGdF_5$:Eu-MW particles were analyzed (Figs. 2c, 2d). As a result, it was found that the $BaGdF_5$:Eu-ST nanoparticles are characterized by dispersion in the range of 4 to 8 nm with the predominant fraction of 6 nm, and the $BaGdF_5$:Eu-MW nanoparticles, in turn, are 6–14 nm in size with the predominant fraction of 10 nm. Thus, the synthesized nanomaterials are suitable in size for the subsequent synthesis of nanocomposites for XPDT.

Results of X-ray fluorescence (XRF) *analysis.* The ratio of metals fused in the synthesis of $BaGdF_5$:Eu-MW is Ba : Gd: Eu $\rightarrow$ 1 : 0.9 : 0.1. The ratio determined using XRF was 1 : 0.9 : 0.08. The deviations from stoichiometry are apparently related to the difference between the ionic radii of gadolinium and the introduced europium ions (the radii of the Gd^{3+} and Eu^{3+} ions are 0.0938 and 0.0947 nm, respectively).

The results of the analysis of the cytotoxicity of the materials. Using the method for assessing the integrity of membranes with trypan blue staining, the toxicity of the synthesized nanomaterial in the experiment was determined *in vitro* on the malignant human cells of the HeLa line (Fig. 3).

The study found that the sample [$BaGdF_5$:Eu-MW] increased the HeLa cell culture's viability by 8% ($p = 0.002$).

The results of the analysis of induction by nanomaterials of generating ROS in cells in vitro. Analysis by the CRO (Fig. 4) and CRG (Fig. 5) channels was carried out with normalization by cell size (FSC channel, the area under the curve; the nCRO and nCRG parameters, respectively) and only in the region of the positive signal of the target probes (CRO^+ and CRG^+ gates, respectively), i.e., with analytical compensation of the autofluorescence. The use of such an algorithm makes it possible to increase the analytical sensitivity and specificity of the method and compensate the differences between the signal level and the actual functional parameters of cells of a different size.

In the quantitative analysis, the median signal level was used as a numerical parameter—as the most representative parameter with the potential qualitative and quantitative effects of the nanoagent on the physiological parameters of the cells.

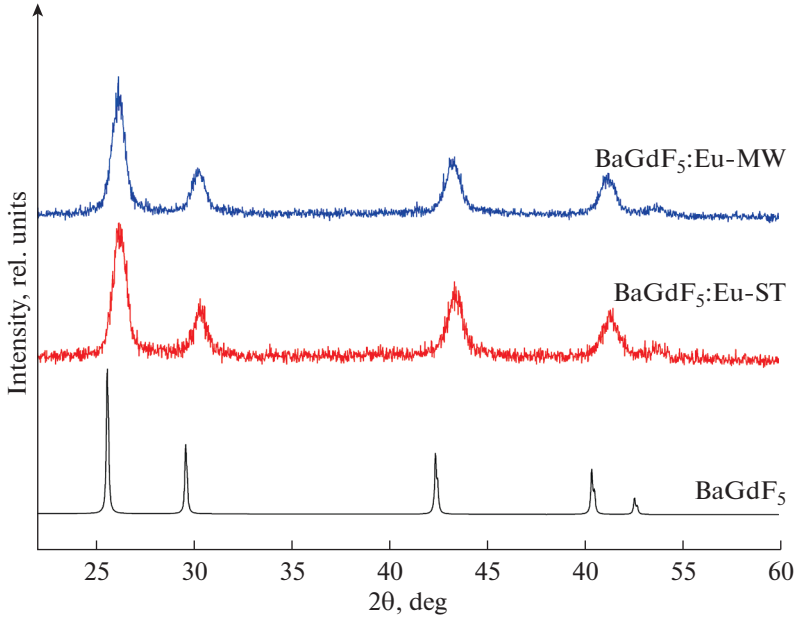

Fig. 1. (Color online) X-ray powder diffraction profiles of synthesized $BaGdF_5$:Eu-ST and $BaGdF_5$:Eu-MW samples. For comparison, the $BaGdF_5$ profile from the PDF-2 database is shown (no. 24-0098).

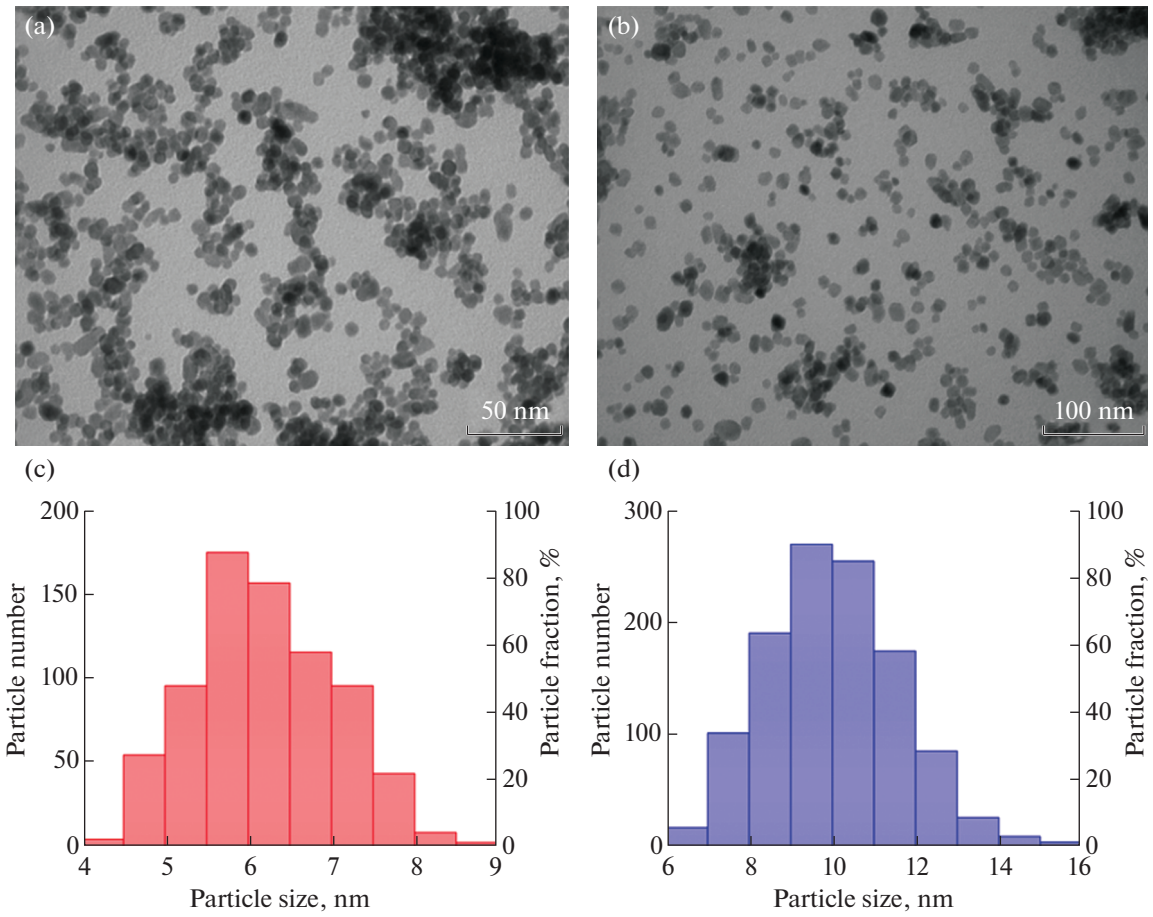

Fig. 2. (Color online) TEM images of $BaGdF_5$:Eu-ST and $BaGdF_5$:Eu-MW samples (a, b); particle size distribution of $BaGdF_5$:Eu-ST and $BaGdF_5$:Eu-MW according to TEM (c, d).

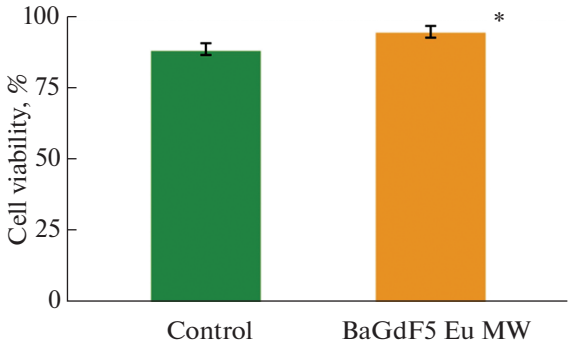

Fig. 3. (Color online) The viability of HeLa cells in the control and after exposure to synthesized nanoagents at the final concentration of 50 μg/mL for 24 h. Error bars correspond to standard deviation. * are statistically significant differences, $p = 0.002$.

As can be seen from the nature of the histograms in the CRO channel (ROS cytosol levels), the control and experimental groups have some differences in the character of the effect on individual cell populations: the histogram peaks in the experimental group are narrower, with the characteristic shift in the cell populations towards an increase in the signal.

The CRG channel study confirmed the qualitative differences observed between the study groups in the CRO channel; in this case the differences were much more pronounced.

The quantitative analysis showed that the studied groups really have pronounced differences in the parameters of the oxidative status of the model line

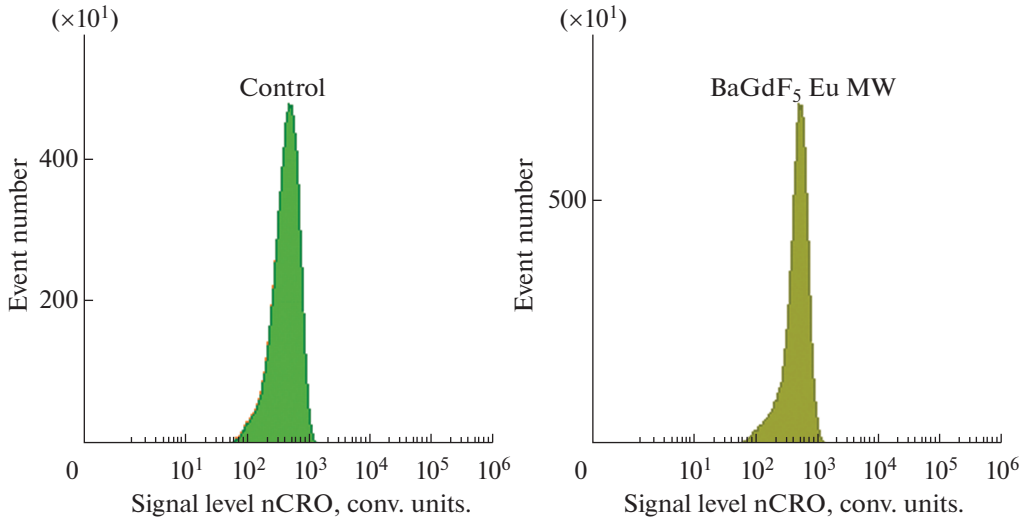

Fig. 4. (Color online) Examples of histograms of the distribution of cells by nCRO+ signal intensity (normalized by cell size ROS cytosol levels) of K562 cells in the control and after exposure to synthesized nanoagents at the final concentration of 50 μg/mL for 1 h.

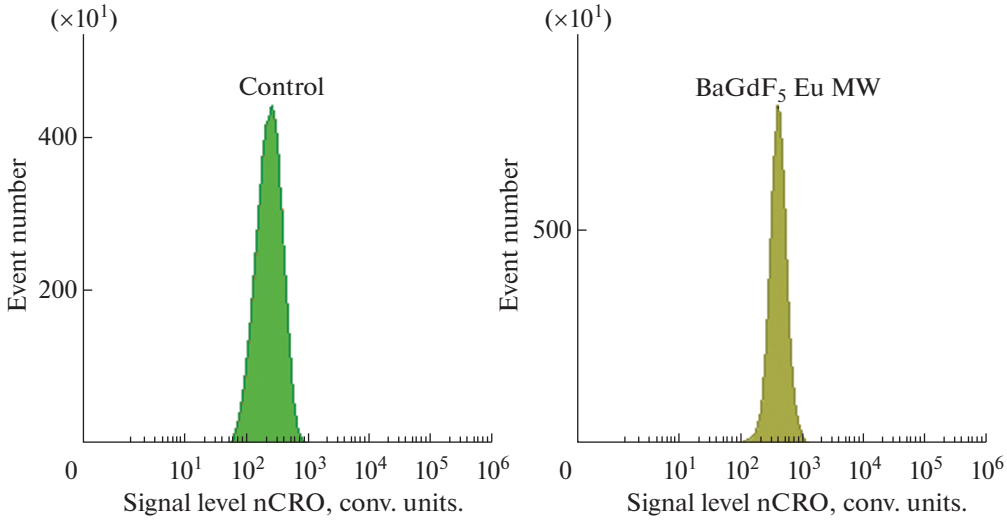

Fig. 5. (Color online) Examples of histograms of cell distribution by nCRG+ signal intensity (normalized to cell size ROS levels of mitochondria and nuclei) of K562 cells in the control and after exposure to synthesized nanoagents at the final concentration of 50 μg/mL for one hour.

Table 2. Normalized intensity of CRO and CRG signals in cells after exposure to a nanoagent for one hour and in control

Group	Analyzed parameter			
	CRO channel		CRG Channel	
	M ± SD*, arb. units	pMW**	M ± SD, arb. units	pMW
Control	462.6 ± 53.31		264.67 ± 36.97	
$BaGdF_5$:Eu-MW	507.6 ± 14.77	0.065	421.75 ± 22.31	0.002

*Mean and standard deviation.

**Significance level according to the Mann–Whitney test.

cells, primarily in the generation of ROS in the nucleus and mitochondria (Table 2).

Although the differences in the production of ROS in the cytosol only approached the threshold of significance, in the DNA-containing organelles, the production of ROS increased by about 60%.

As a result of the cytotoxicity studies, the prospects for the further use of $BaGdF_5$:Eu-MW nanoparticles were established even without a coating. Moreover, the nanoagent was not simply not toxic but it statistically significantly increased cell viability by almost 8%. As a rule, such a picture is observed upon stimulation by the active agent of the protective cascades of the cell.

In this respect, the ROS-inducing ability of the nanoagent was studied by flow cytometry. During this experiment, the K562 cells were incubated for one hour together with the nanoparticles—this is the standard induction time of the primary ROS wave under the action of redox-active agents. As a result of the study, it was found that a slightly increased ROS induction in the cytosol was indicative of the ability of the studied nanoagent to stimulate cell defense systems against the background of a significant increase in the ROS of the DNA-containing organelles. Such a picture testifies to the classical variant of differential activation of a cell's defense systems. Moreover, this difference in physiological activity is interesting in that the cytosolic protective systems of the cells respond much more weakly than is actually required due to the lower degree of the ROS induction of the cytosol and the much more limited spectrum of the sensors of the ROS in the nucleus and mitochondria compared to cytosol. As a result, such agents are capable of causing effective damage to the DNA of the nucleus and mitochondria and causing cell death by various mechanisms—from metabolic catastrophe to necrosis and autoschisis—against the background of the introduction of additional damage to the DNA of cells even in the case of the intensified work of their antioxidant systems.

Thus, the ability described for $BaGdF_5$:Eu-MW to induce the generation of the ROS in DNA-containing organelles after penetration into cells is one of the most important parameters of nanoparticles for biomedical applications. Information on this property of the synthesized nanoagent allows, on the one hand, to develop a protocol for the early adaptation of non-malignant body cells (different from malignant ones in their ability to respond to prooxidant changes in the oxidative status) and, on the other hand, to use the identified properties as an additional therapeutic modality in XPDT.

CONCLUSIONS

The application of the standard solvothermal method and the technique using microwave radiation leads to obtaining $BaGdF_5$ nanoparticles 6–14 nm in size that resemble each other in their structural data. However, when using microwave radiation, the time of the synthesis is reduced by at least an order of magnitude. According to their dimensional characteristics, these nanoparticles comply with the requirements for the subsequent production of nanocomposites based on them for XPDT. The synthesized $BaGdF_5$:Eu-MW nanoparticles are completely biocompatible and do not have a material negative effect on the viability of the HeLa and K562 cell lines.

FUNDING

The study was financed by the Russian Science Foundation (project no. 19-15-00305).

REFERENCES

1. M. Malvezzi, P. Bertuccio, F. Levi, et al., Ann. Oncol. **23**, 1044 (2012).
2. D. Ashen-Garry and M. Selke, Photochem. Photobiol. **90**, 257 (2014).
3. E. Abliz, J. E. Collins, H. Bell, and D. B. Tata, X-Ray Sci. Technol. **19**, 521 (2011).
4. Y. Yang, S. Karakhanova, J. Werner, and A. V. Bazhin, Curr. Med. Chem. **20**, 3677 (2013).
5. A. A. Sapre, E. Novitskaya, V. Vakharia, et al., Mater. Lett. **228**, 49 (2018).
6. S. Mordon, C. Cochrane, J. B. Tylcz, et al., Photodiagn. Photodyn. Ther. **12**, 1 (2015).
7. A.-L. Bulin, C. Truillet, R. Chouikrat, et al., J. Phys. Chem. C **117**, 21583 (2013).

8. M. H. Chen, Y. J. Jenh, S. K. Wu, et al., Nanoscale Res. Lett. **12**, 62 (2017).
9. H. Guan, Y. Sheng, Y. Song, et al., RSC Adv. **6**, 73160 (2016).
10. H. Li, G. Liu, J. Wang, et al., J. Lumin. **186**, 6 (2017).
11. A. C. Yanes, J. Castillo, and E. Ortiz, J. Alloys Compd. **773**, 1099 (2019).
12. X. Huang, L. Jiang, X. Li, and A. He, J. Alloys Compd. **721**, 374 (2017).
13. A. I. Becerro, D. Gonzalez-Mancebo, E. Cantelar, et al., Langmuir **32**, 411 (2016).
14. S. Hao, G. Chen, and C. Yang, Theranostics **3**, 331 (2013).
15. M. R. Hamblin, Dalton Trans. **47**, 8571 (2018).
16. R. D. Teo, J. Termini, and H. B. Gray, J. Med. Chem. **59**, 6012 (2016).
17. D. Yang, Y. Dai, J. Liu, et al., Biomaterials **35**, 2011 (2014).
18. T. Grzyb, L. Mrowczynska, A. Szczeszak, et al., J. Nanopart. Res. **17**, 399 (2015).
19. V. V. Bakhmetyev, A. M. Dorokhina, M. V. Keskinova, et al., Chem. Papers **74**, 787 (2019).
20. L. Sudheendra, G. K. Das, C. Li, et al., Chem. Mater. **26**, 1881 (2014).
21. International Centre for Diffraction Data (ICDD). Database PDF-2, Card No. 24-0098. www.icdd.com/.
22. V. V. Butova, V. A. Polyakov, E. A. Bulanova, et al., Microporous Mesoporous Mater. **293** (2020).
23. V. V. Butova, K. S. Vetlitsyna-Novikova, I. A. Pankin, et al., Microporous Mesoporous Mater. **296** (2020).
24. D. Yu. Kirsanova, Z. M. Gadzhimagomedova, A. Y. Maksimov, and A. V. Soldatov, "Nanomaterials for deep tumor treatment," (2020, in press).
25. Z. M. Gadzhimagomedova, O. I. Kit, P. V. Zolotikhin, et al., "Nanocomposites for X-ray photodynamic therapy," (2020, in press).

SPELL: OK